円盤の振動・波動現象

加藤正二

2019年8月23日 福山

Helioseismology

５分振動の発見 *(Leigthon et al. 1962)*

太陽の内部構造・回転則の解明

Astroseismology

Discoseismology (simeq 1980)

中心天体の解明

特徴： configuration

rotation の重要性

wave energy (positive and negative)

GR の重要

励起機構の多様性

目次

* 観測事実の short review
  HFQPOs in black-hole objects, kHz QPOs in neutron stars
  QPOs in galactic nuclei, V/R variations in Be stars
* 円盤振動の基本的性質
  (horizontal) epicyclic frequency, vertical epicyclic frequency
  effects of general relativity, separation of propagation regions
  trapping of oscillations
  positive and negative wave energy
* 円盤振動の分類
  p-mode, g-mode (r-mode),
  c-mode (corrugation mode, vertical p-mode
  Rossby-type mode
* 円盤振動の励起機構
  viscous overstability, corotation resonance
  wave-wave resonant instability, turbulent excitation
* wave-wave resonant instability の応用
  superhumps,
  excitation of trapped g-mode oscillations
  high frequency quasi-periodic oscillations (HFQPOs)

1. Observational Evidence Suggesting the Presence of Disk Oscillations

- High Frequency Quasi-Periodic Oscillations

  NS binaries
    KHz QPOs
      特徴： pair あり， correlated change (not 3 : 2)
    Hectohertz QPOs
      特徴： 100Hz 程度、変動小
  BH binaries
    HF QPOs
      特徴： pair あり， 3 : 2

- Superhumps in Dwarf Novae

- V/R variations in Be Stars

Twin kHz QPOS

hectohertz QPOs

HFQPOs in BH binaries

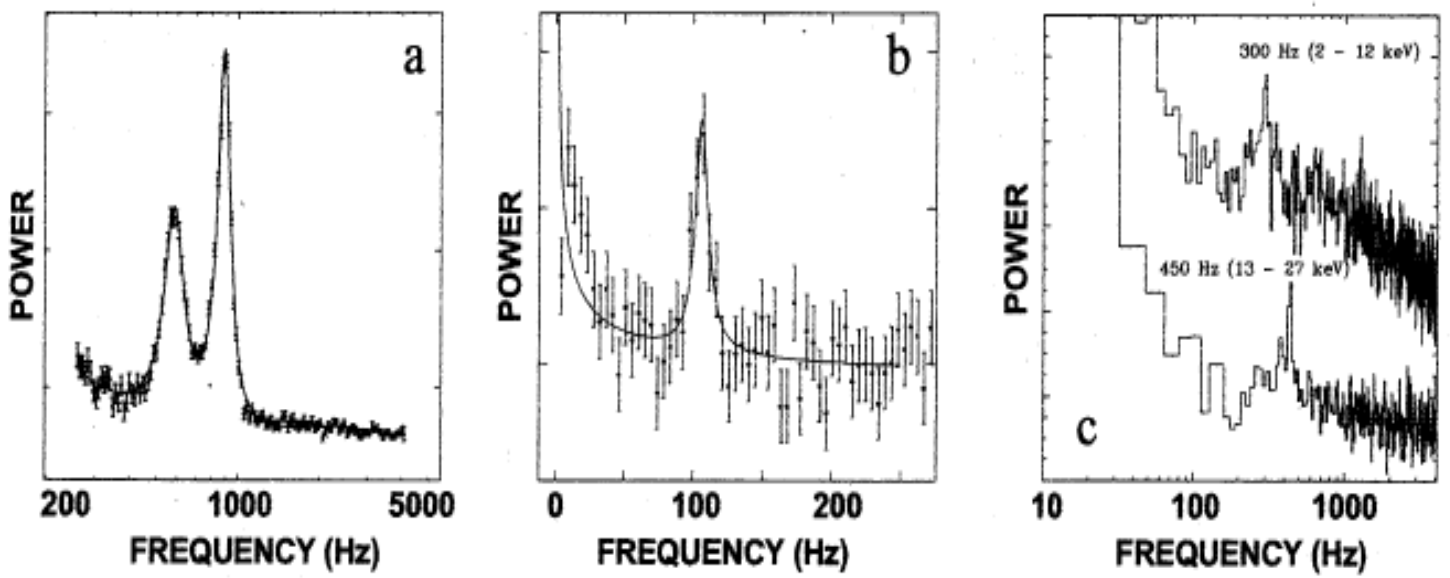

Various high-frequency QPOs in X-ray binaries. (a) Twin kHz QPOs in Sco X-1 (van der Klis et al. 1997), (b) hectohertz QPO in 4U 0614+09, (c) HFQPOs in GRO J1655-40 (Strohmayer 2001a).In panel (c), the lower curve is the power in the energy range of 13-27 keV and a QPO can be seen at 450 Hz, while the upper curve is the power in the range of 2-12 keV and a QPO is seen at 300 Hz. (After van der Klis 2004, in "Compact Stellar X-ray Sources", eds. W.H.G. Lewin and M. van der Klis (Cambridge University Press; Cambridge), 39

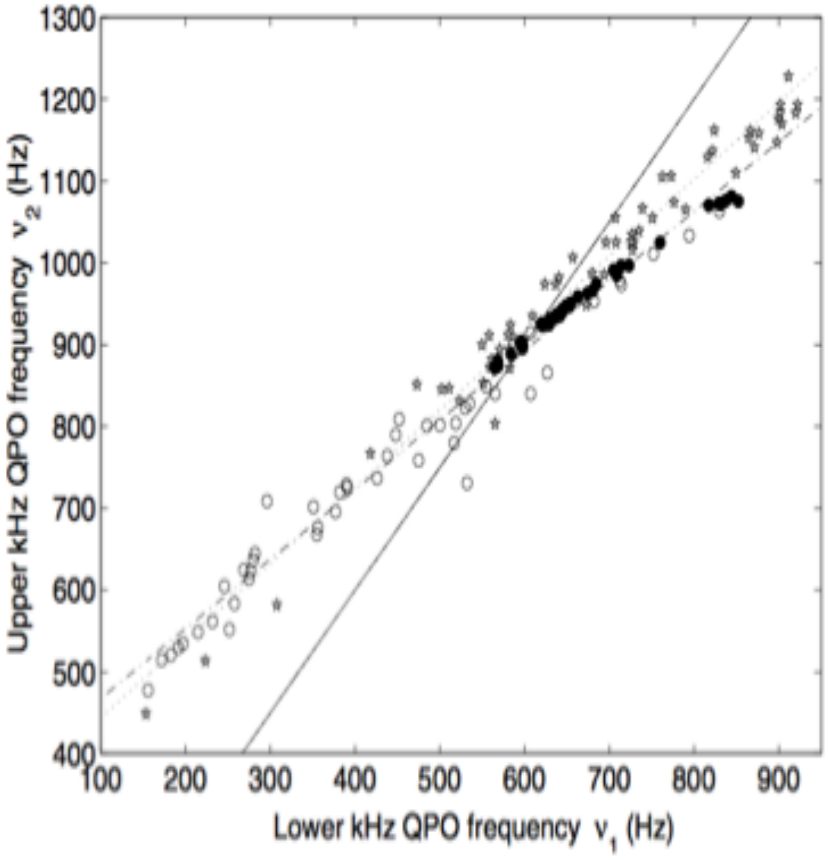

Frequency correlation between lower and upper kHz QPO frequencies for the Sco X-1 (filled circles), for Z sources (open circles) and for Atoll sources (stars). The dotted line is the best linear fit to the Atoll points, the dot-dashed line is the best linear fit to the Z sources (excluding Sco X-1), and the thick line represents a fixed 3 : 2 ratio. (After T. Belloni, M. Méndez, & J. Homan, 2005, A&A 437, 209,

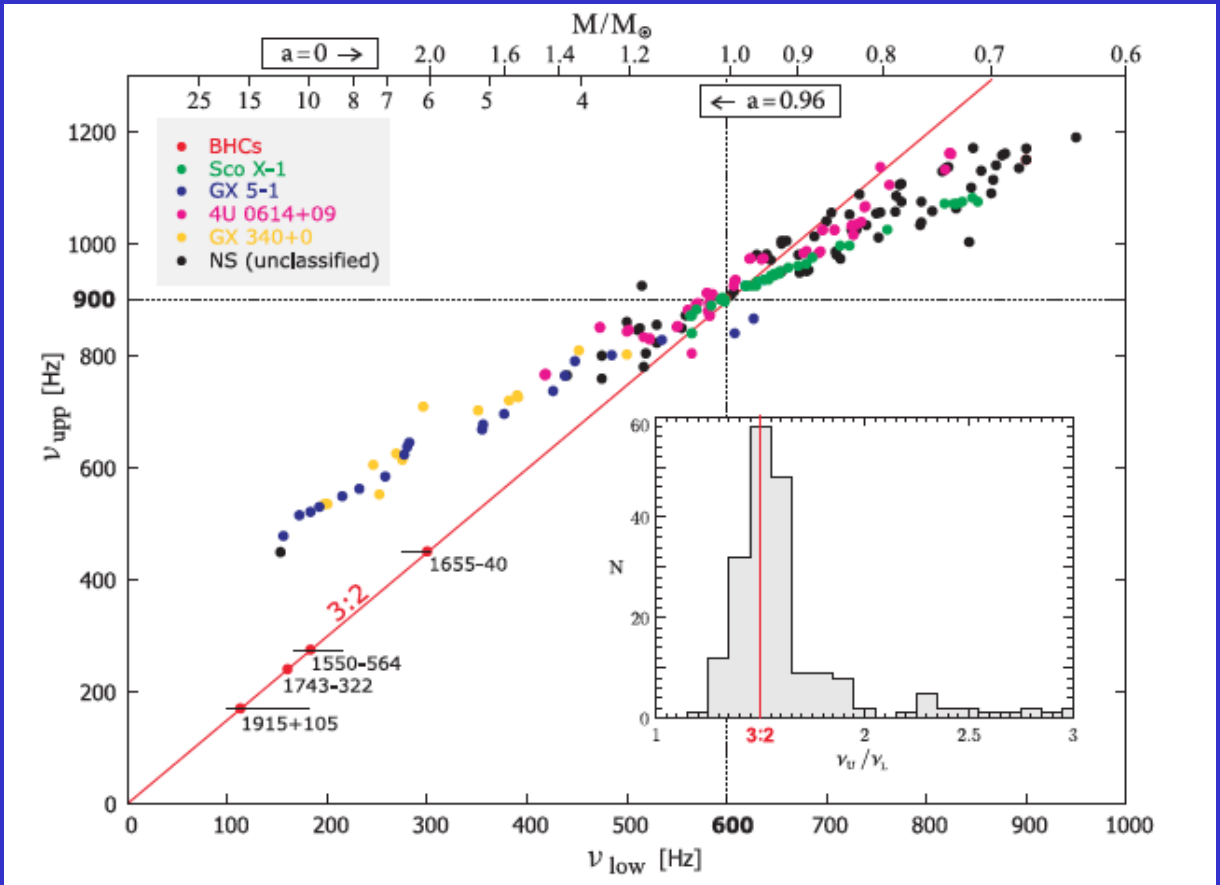

Abramowicz, M. A. 2004, Astron. Nachr./AN 325

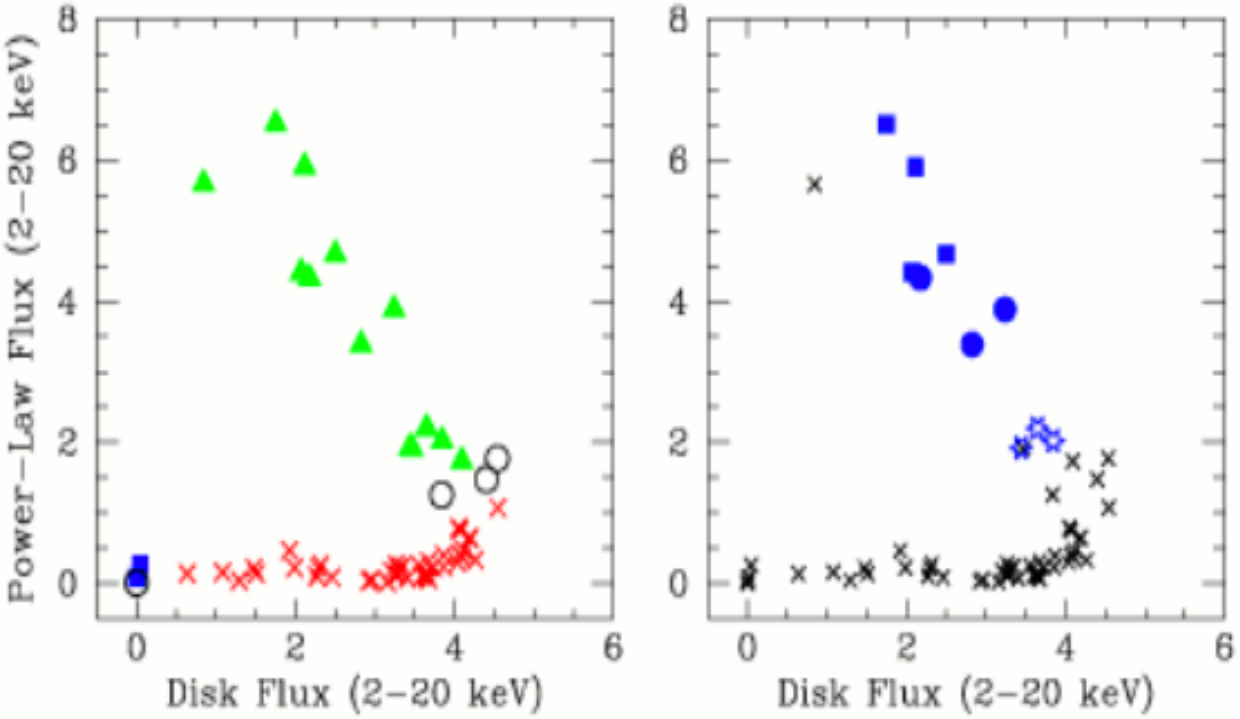

X-ray states and HFQPOs during 1996-1997 outburst of GRO J1655-40. The left panel shows the energy diagram, where flux from the accretion disk is plotted versus flux from the power-law component. Here, the symbol type denotes the X-ray state: thermal (X), hard (square), steep power-law state (triangle), any type of intermediate state (circle). The right panel shows the same data points, while the symbol choice denotes HFQPOs detections: 300 Hz (square), 450 Hz (star), both HFQPOs (circle), and no HFQPOs (X). The HFQPOs detections are clearly linked to the steep power-low state, and the HFQPO frequency is clearly correlated with power-law luminosity. (Color online) (After Remillard 2005, Astron. Nachr. 326, 804,

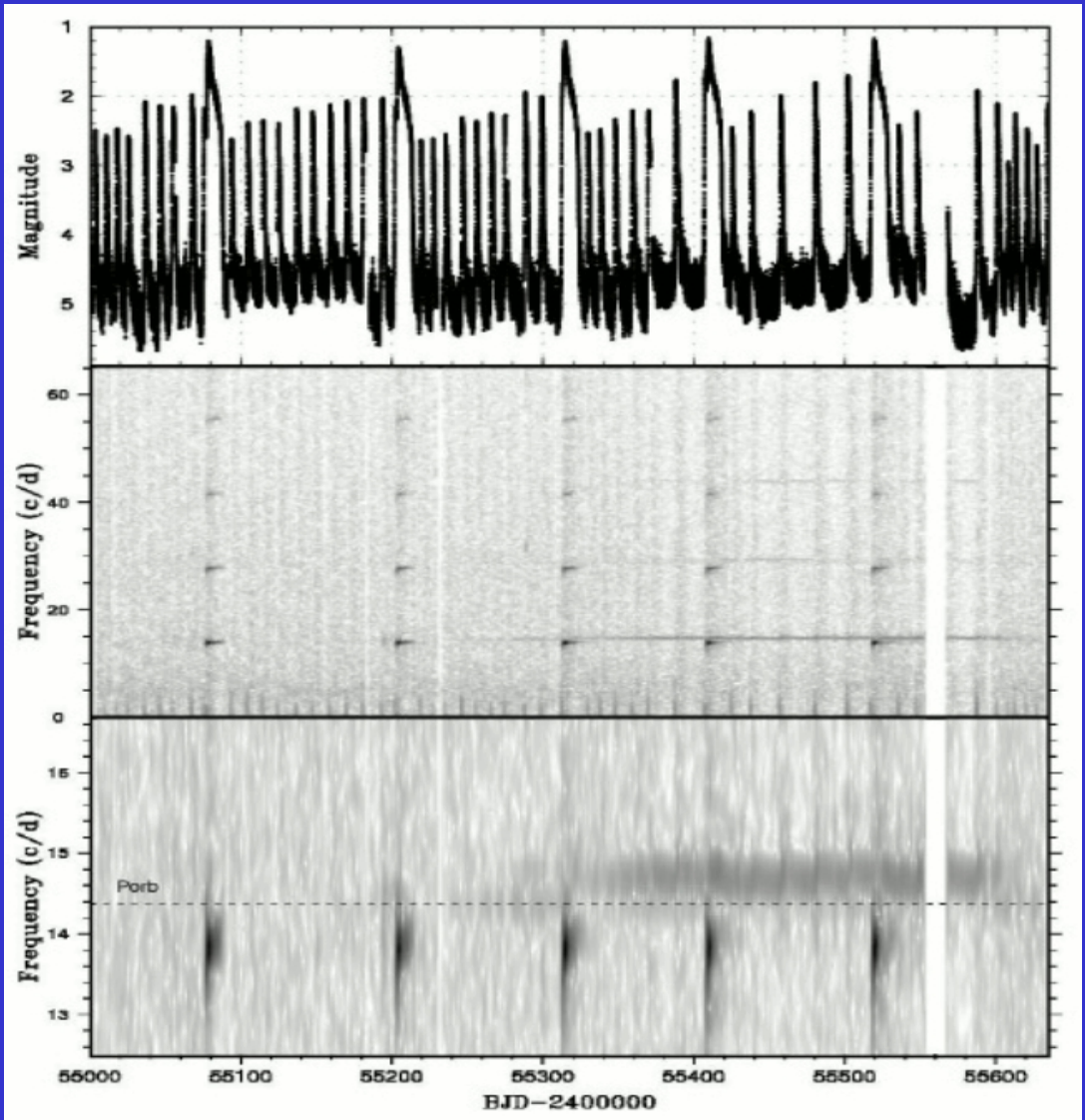

After Osaki and T.Kato 2013, Publ. A.S. Japan 65, 59

γ Cas

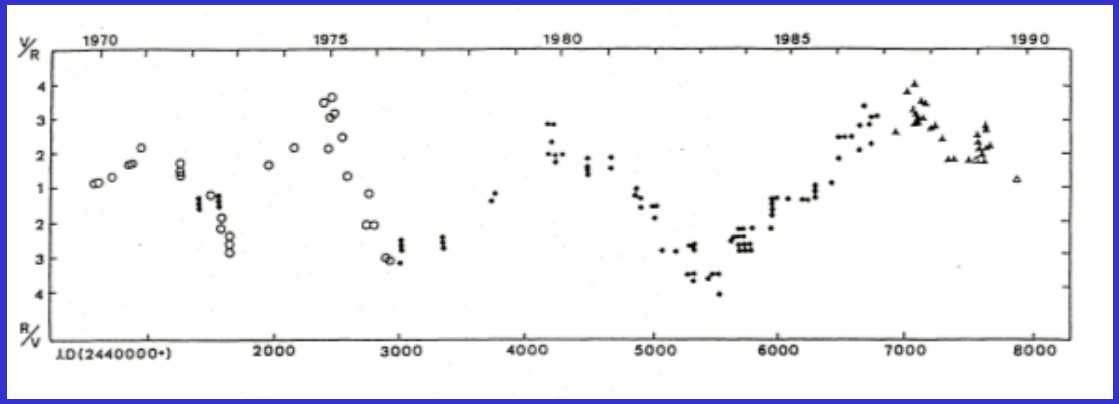

Fig. 1.6 Long-term variations of γ Cas in 1969-1989 (Adapted from T. Horaguchi, T. Kogure, R. Hirata, et al. 1994, PASJ, 46, 9,

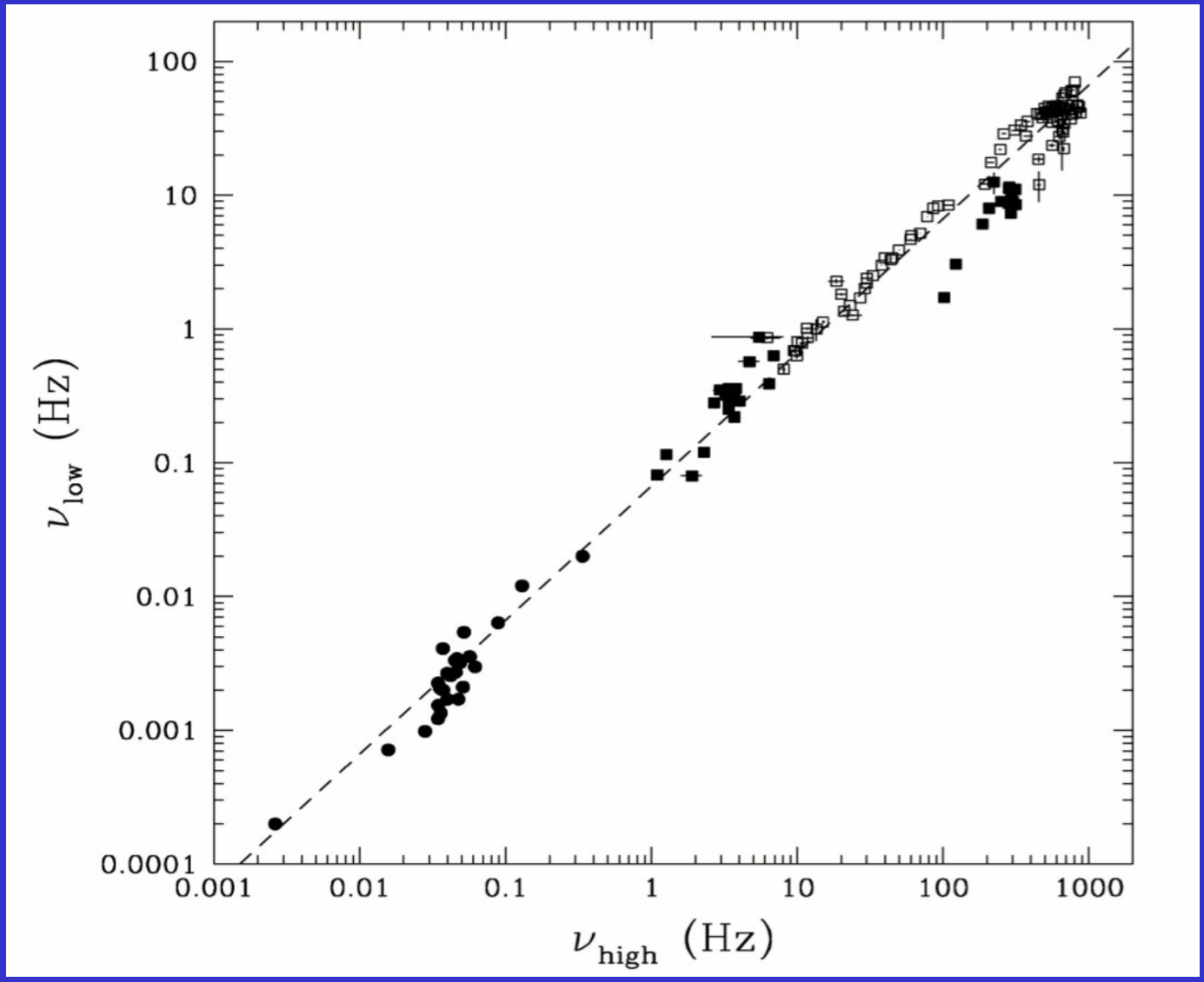

Frequency correlation between the high and low QPOs from CVs to X-ray binaries. The filled circles are for CVs, the open squares are for neutron-star binaries, and the filled squares are for black-hole binaries. (After B. Warner, P.A. Woudt, & M.L. Pretorius, 2003, MNRAS 344, 1193,

２．円盤振動を考える上での基礎量および基礎概念

○ 回転に伴う restoring force

Epicyclic frequency

○ corotation resonance and Lindblad resonances

○ Lagrangian representation of waves の重要性

Hermitian operator
Wave energy

Epicyclic frequency

$$\frac{d^2r}{dt^2} = -\frac{d\psi_{\rm eff}}{dr}$$

$$\psi_{\rm eff}(r) = -\frac{GM}{r}\left(1+\frac{\ell^2}{c^2r^2}\right)+\frac{\ell^2}{2r^2}$$

$$\ell = \text{const.}$$

$$\frac{d^2\xi}{dt^2} = -\left(\frac{d^2\psi_{\rm eff}}{dr^2}\right)\xi$$

$$\frac{d^2\psi_{\rm eff}}{dr^2} = \left(1-\frac{r_{\rm g}}{r}\right)\frac{GM/r^2}{r-3r_{\rm g}/2}$$

$$r_{\rm g} = \frac{2GM}{c^2}$$

$$\left(1-\frac{3r_{\rm g}}{2r}\right)^{-1/2},$$

red shift factor

$$\kappa^2 = \frac{GM}{r^2}\left(1-\frac{3r_{\rm g}}{r}\right)$$

Fukue 1980
Aliev, Galtsov 1981
Okazaki 1987

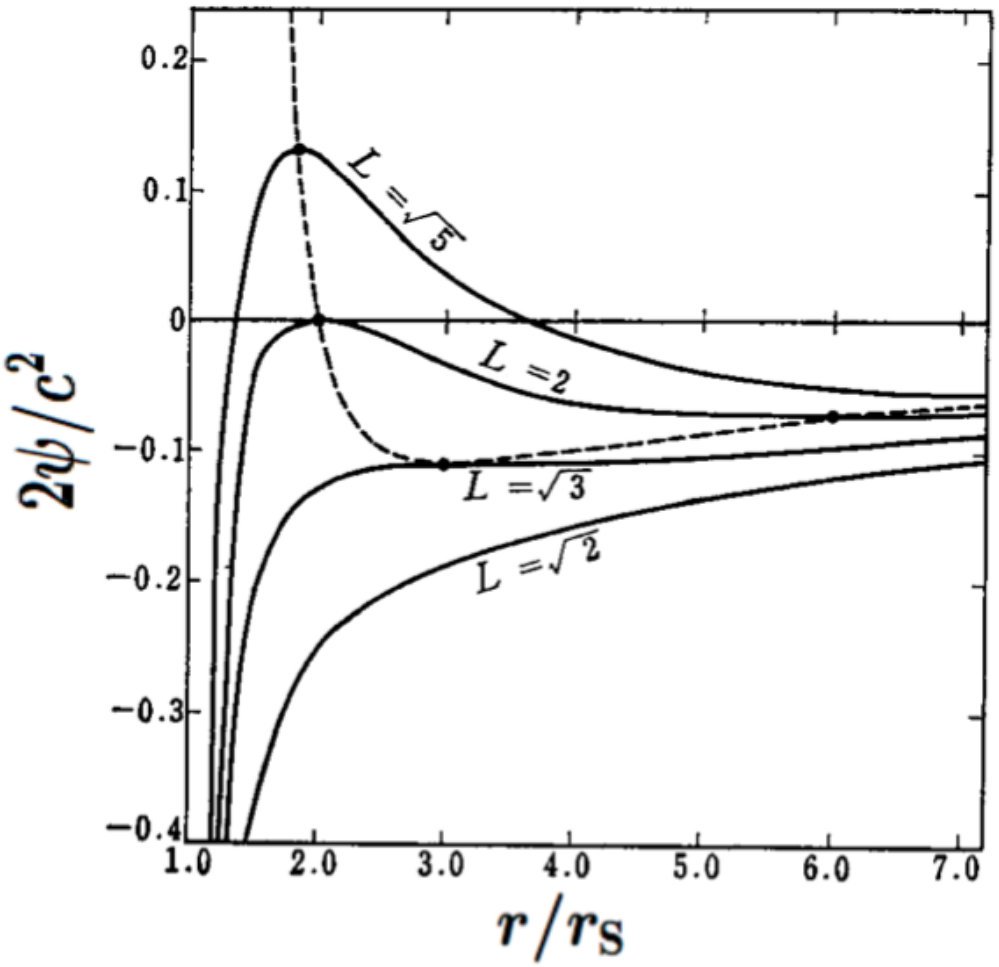

Effective potential for circular motions in the Schwarzschild metric. The radial dependence of the effective potential $\psi(r)$ is shown for some values of L. In the case where L is large, the effective potential $\psi(r)$ has a maximum and a minimum. As L decreases these two radii approach and finally merge for $L < \sqrt{3} r_S c$, and there is no minimum and maximum. The dotted curve shows the loci of the maximum and minimum points.

$$\kappa_{\rm GR}^2 = \frac{GM}{r^2}\frac{1 - 3r_{\rm g}/r \pm 8a_*(r_{\rm g}/2r)^{3/2} - 3a_*^2(r_{\rm g}/2r)^2}{[1 \pm a_*(r_{\rm g}/2r)^{3/2}]^2},$$

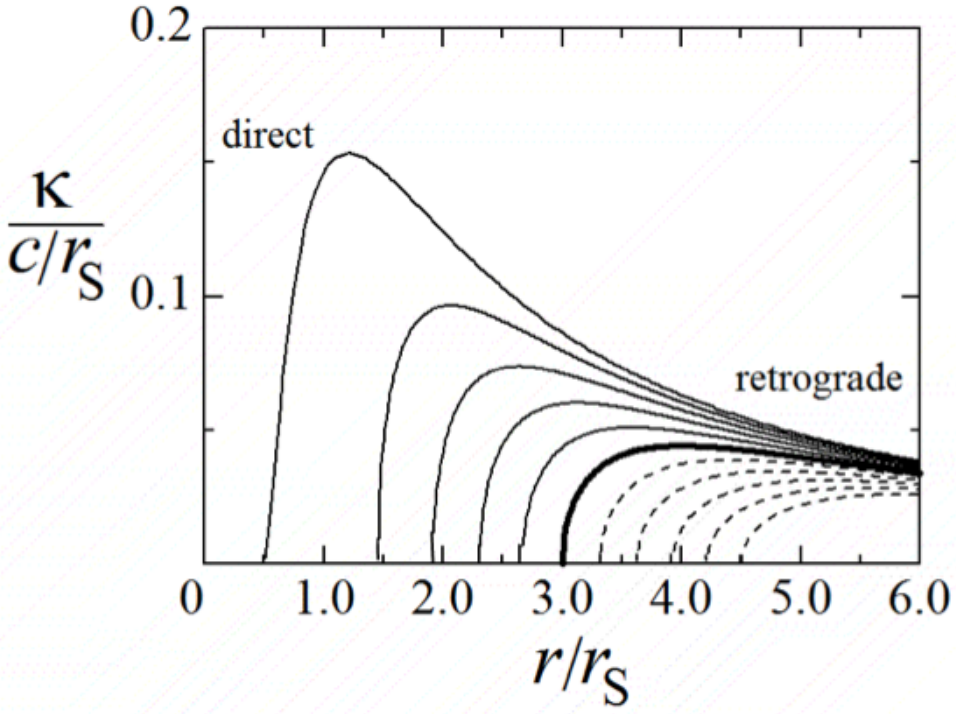

Fig. 9.6 Radial dependence of epicyclic frequency, $\kappa(r)$. $a_* = 0$ shows the case of the Schwarzschild metric (thick curve). The dotted curves denote the cases of $a_* < 0$ (retrograde rotation).

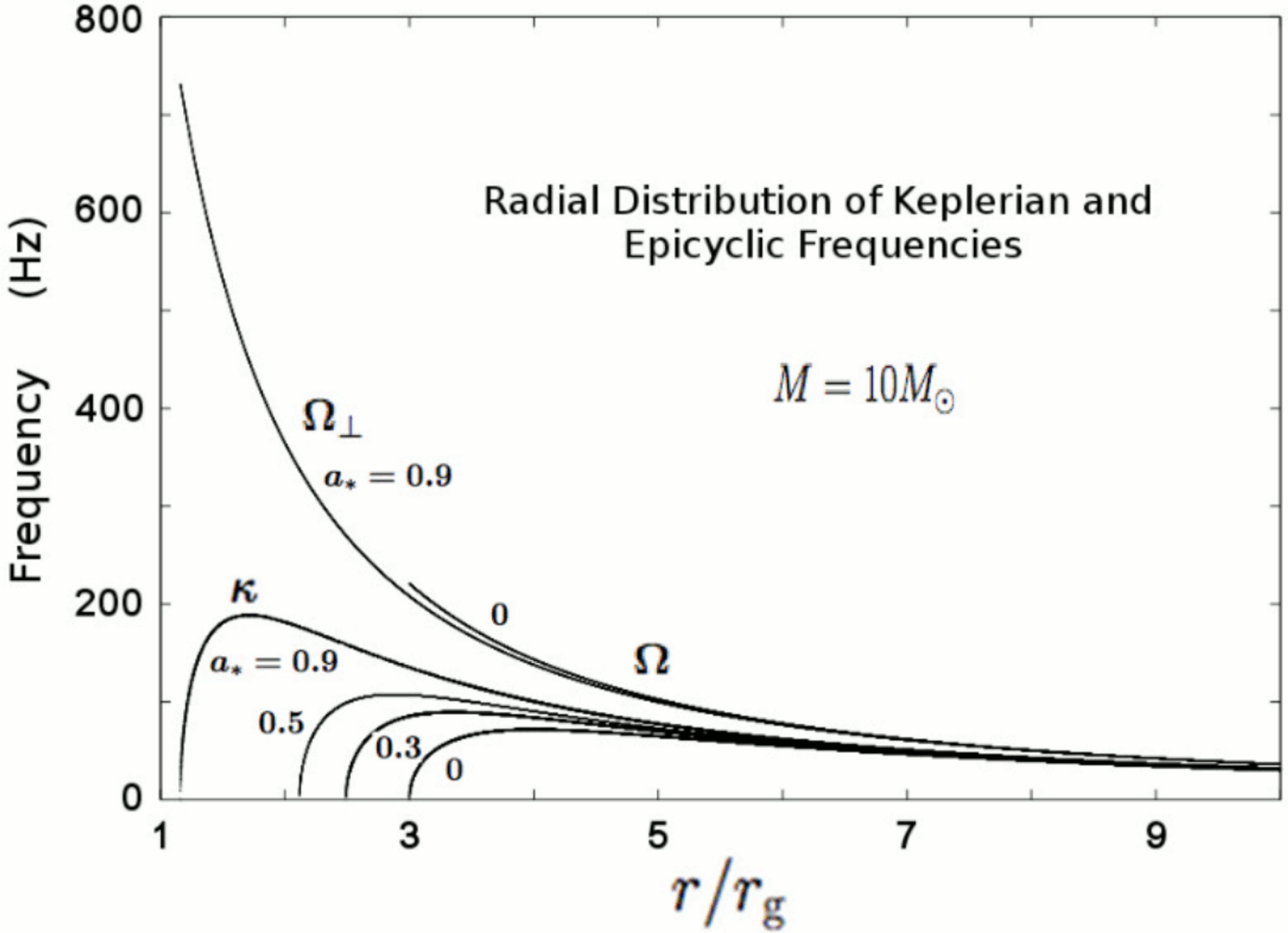
Radial Distribution of Keplerian and
Epicyclic Frequencies
$M = 10M_\odot$
Frequency (Hz)
800
600
400
200
0
1
3
5
7
9
r/r_g
$\Omega_\perp$
$a_* = 0.9$
κ
$a_* = 0.9$
0.5
0.3
0
0
Ω

Corotation resonance and Lindblad resonances

$$\exp[i(\omega t - m\varphi)]$$

Corotation resonance:

phase velocity in azimuthal direction = ang. of rotation

$$\omega/m = \Omega \quad or \quad \omega = m\Omega$$

Lindblad resonances:

$$\omega/m = \Omega \pm \kappa/m \quad or \quad \omega = m\Omega \pm \kappa$$

Wave energy of oscillations

$$E(t) = \int \rho_0 \left[\int_{-\infty}^{t} \frac{\partial \boldsymbol{\xi}}{\partial t} \delta \boldsymbol{f} \, dt \right] dV.$$

$$\frac{\partial \boldsymbol{\xi}}{\partial t} \left(\rho_0 \frac{\partial^2 \boldsymbol{\xi}}{\partial t^2} + 2\rho_0 (\boldsymbol{u}_0 \cdot \nabla) \frac{\partial \boldsymbol{\xi}}{\partial t} + \boldsymbol{L}(\boldsymbol{\xi}) \right)$$

$$E = \frac{1}{2} \int \rho_0 \left[\left(\frac{\partial \boldsymbol{\xi}}{\partial t} \right)^2 + \boldsymbol{\xi} \cdot \boldsymbol{L}(\boldsymbol{\xi}) \right] dV.$$

$$\frac{\partial \boldsymbol{E}}{\partial \boldsymbol{t}} = \boldsymbol{0}$$

$$E = \frac{1}{2} \int \rho_0 \omega (\omega - m\Omega) (\breve{\xi}_r^* \breve{\xi}_r + \breve{\xi}_z^* \breve{\xi}_z) dV.$$

$$\boldsymbol{E < 0} \quad \textbf{for} \quad \boldsymbol{\omega < m\Omega}$$

$$\boldsymbol{E > 0} \quad \textbf{for} \quad \boldsymbol{\omega > m\Omega}$$

Lagrangian Description of Oscillations

Lynden-Bell, Ostriker 1967

$$\frac{D_0^2\boldsymbol{\xi}}{Dt^2} = \delta\left(-\nabla\psi - \frac{1}{\rho}\nabla p\right),$$

$$\delta\left(\frac{D\boldsymbol{v}}{Dt}\right) = \frac{D_0}{Dt}\delta\boldsymbol{v} = \frac{D_0^2}{Dt^2}\boldsymbol{\xi}.$$

$$\frac{D_0}{Dt} = \frac{\partial}{\partial t} + \boldsymbol{u}_0\cdot\nabla.$$

$$\delta\rho + \rho_0 \mathrm{div}\boldsymbol{\xi} = 0.$$

$$\delta p = c_s^2\delta\rho = \Gamma_1\frac{p_0}{\rho_0}\delta\rho,$$

$$\rho_0\frac{\partial^2\boldsymbol{\xi}}{\partial t^2} + 2\rho_0(\boldsymbol{u}_0\cdot\nabla)\frac{\partial\boldsymbol{\xi}}{\partial t} + \boldsymbol{L}(\boldsymbol{\xi}) = 0,$$

$$\boldsymbol{L}(\boldsymbol{\xi}) = \rho_0(\boldsymbol{u}_0\cdot\nabla)(\boldsymbol{u}_0\cdot\nabla)\boldsymbol{\xi} + \rho_0(\boldsymbol{\xi}\cdot\nabla)(\nabla\psi_0) + \nabla\left[(1-\Gamma_1)p_0\mathrm{div}\boldsymbol{\xi}\right]$$
$$-p_0\nabla(\mathrm{div}\boldsymbol{\xi}) - \nabla[(\boldsymbol{\xi}\cdot\nabla)p_0] + (\boldsymbol{\xi}\cdot\nabla)(\nabla p_0).$$

$$\boldsymbol{\xi} = \Re[\hat{\boldsymbol{\xi}}\exp(i\omega t)] = \Re\left[\breve{\boldsymbol{\xi}}\exp[(i\omega t - im\varphi)]\right]$$

wave equation

$$-\omega^2\rho_0\hat{\boldsymbol{\xi}} + 2i\omega\rho_0(\boldsymbol{u}_0\cdot\nabla)\hat{\boldsymbol{\xi}} + \boldsymbol{L}(\hat{\boldsymbol{\xi}}) = 0,$$

$\mathcal{L}$ is Hermitian (self-adjoint operator)

$$\int \hat{\boldsymbol{\eta}}^*\cdot\boldsymbol{L}(\hat{\boldsymbol{\xi}})dV = \int \hat{\boldsymbol{\xi}}^*\cdot\boldsymbol{L}(\hat{\boldsymbol{\eta}})dV,$$

This characteristic is extended to cases of MHD perturbations

3. Classification of Disk Oscillations and Trapping

円盤振動モードの分類

Local 近似

$$\tilde{\omega} = \omega - m\Omega,$$

$$k^2\tilde{\omega}^2 c_{\rm s}^2 = (\tilde{\omega}^2 - \kappa^2)(\tilde{\omega}^2 - n\Omega_\perp^2).$$

$n = 0:$	$\tilde{\omega}^2 = c_{\rm s}^2 k^2 + \kappa^2$	inertial acoustic mode
$n \neq 0:$	$\tilde{\omega}^2 > n\Omega_\perp^2$	vertical p-mode
	$\tilde{\omega}^2 < \kappa^2$	g-mode (r mode)

Table 4.1 Classification of Disk Oscillation Modes

	node number in the vertical direction		
frequency	$n = 0$	$n = 1$	$n \geq 2$
higher $\tilde{\omega}^2$	p-mode (inertial-acoustic mode)	c-mode (corrugation mode)	vertical p-mode (vertical-acoustic mode)
lower $\tilde{\omega}^2$	none	g-mode (gravity or r-mode)	g-mode (gravity or r-mode)
complex $\tilde{\omega}$	Rossby mode		

$$\tilde{\omega} = \omega - m\Omega,$$

$$k^2\tilde{\omega}^2 c_{\rm s}^2 = (\tilde{\omega}^2 - \kappa^2)(\tilde{\omega}^2 - n\Omega_\perp^2).$$

n=0 p-mode oscillations

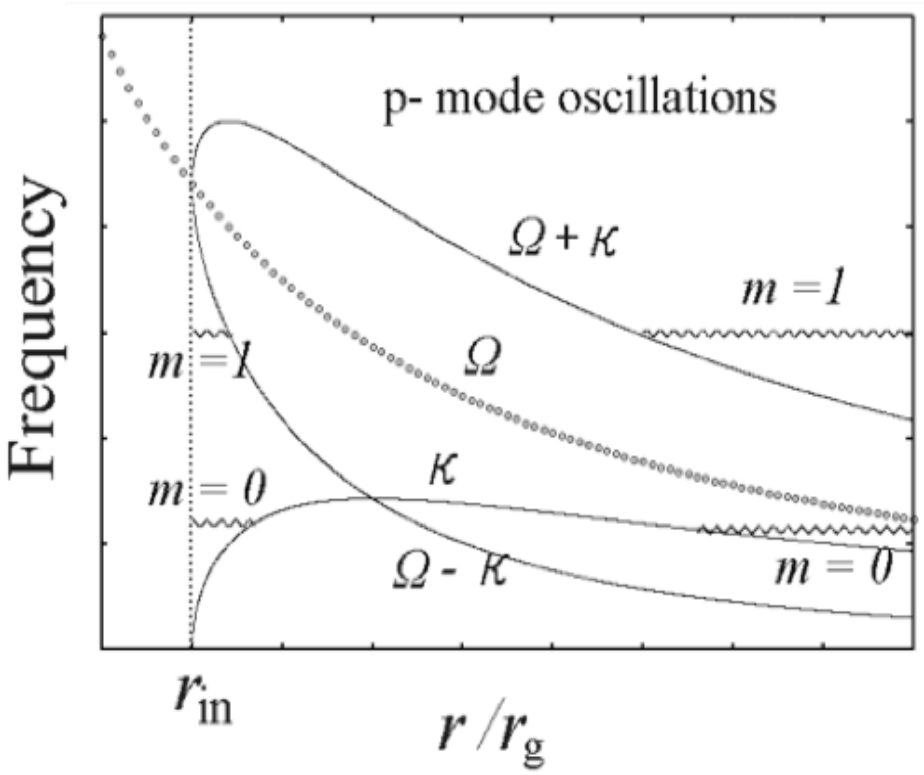

Fig. 6.1 Schematic diagram showing propagation regions of p-mode oscillations ($n = 0$) in relativistic disks. Cases of $m = 0$ and $m = 1$ are shown. The radius, $r_{\rm in}$, is the inner edge of the disks, which will be the radius of ISCO (inner stable circular orbit) in the cases of geometricaly thin disks. $r_{\rm g}$ is the Schwarzscild radius defined by $r_{\rm g} = 2GM/c^2$, where M is the mass of the central object.

n=1 g-mode oscillations

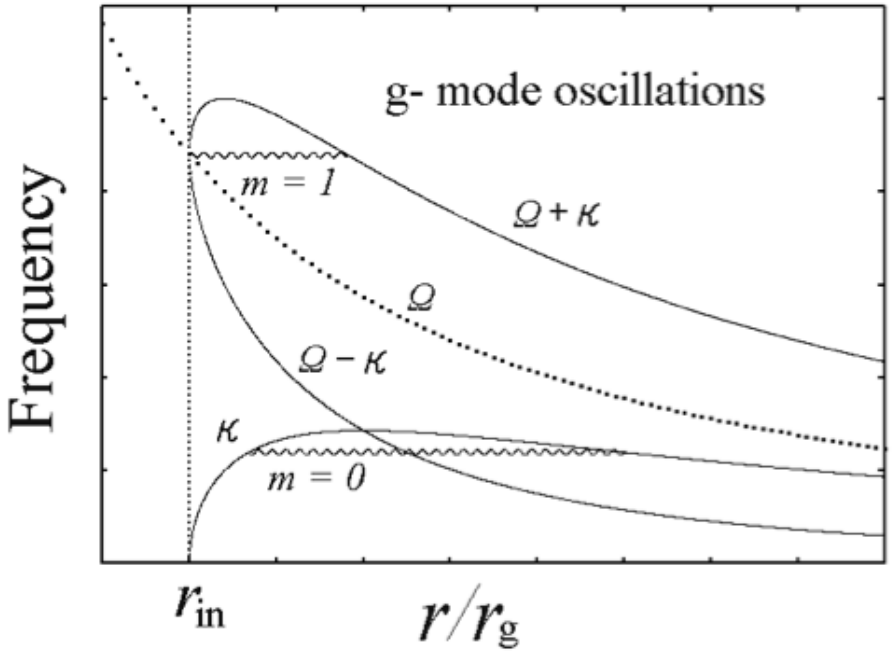

Fig. 1.3 Schematic propagation diagram showing the propagation regions of g-mode oscillations in relativistic disks with no magnetic fields. Cases of $m = 0$ and $m = 1$ are shown with $n = 1$. In the case of non-axisymmetric ($m \neq 0$) oscillations, the radius of corotation resonance ($\omega = m\Omega$) appears in their propagation region, unless ω is in the range of $\Omega_{\rm in} < \omega < (\Omega + \kappa)_{\rm max}$.

n=2 vertical p-mode oscillations

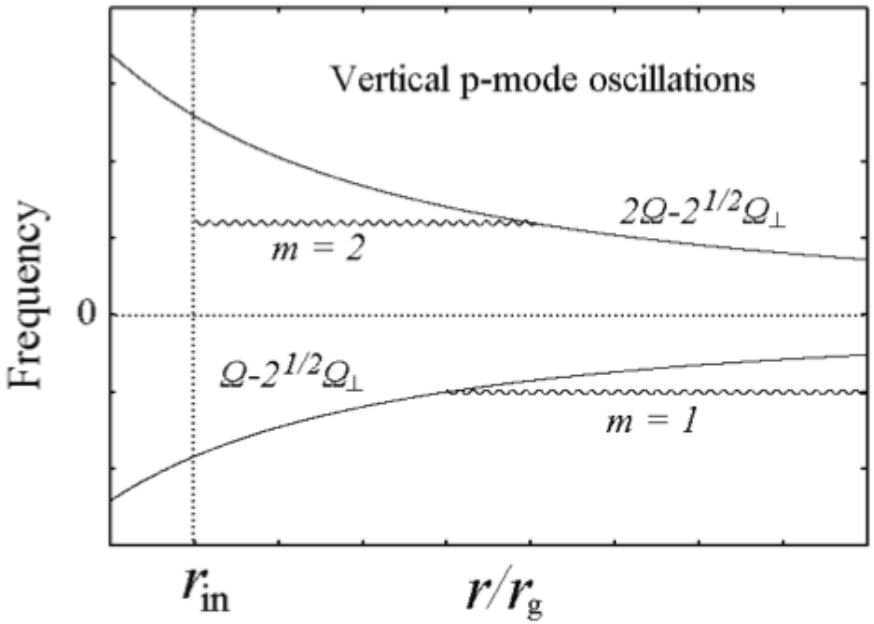

Fig. 1.2 Schematic propagation diagram showing propagation regions of vertical p-modes ($n \geq 2$) oscillations in relativistic disks. Two cases of $m = 1$ and $m = 2$ with $K_n(= n) = 2$ are shown. In the case of $n = 2$ oscillations, one-armed ($m = 1$) oscillations are not trapped, but two-armed ($m = 2$) ones can be trapped in the innermost region of disks. Similar arguments can be made for $n \geq 3$ oscillations. Oscillations with a large n, however, will not be of interest in observational viewpoints.

４．振動の励起機構

- viscous overstability
  Kato 1978
- corotation resonance
  Drury 1985, Papaloizou, Pringle 1984 以下多数
- wave-wave resonant instability in deformed systems
  Kato 2013
  狭義　wave excitation in warped disks
  Kato 2004, 2008, Ferreria, Ogilvie 2008
- turbulent excitation
  星の場合は Goldreich Keeley 1977

Viscous pulsation instability

Thermal pulsation instability と比較

Thermal pulsation instability
　thermal energy flow をmodulate して kinetic energy へ

$$\oint \int \frac{\delta T}{T_0} \delta \left(\epsilon - \frac{1}{\rho} \mathrm{div} \boldsymbol{F} \right) dm > 0,$$

Viscous pulsation instability
　Angular momentum flow に伴う energy を kinetic energy へ

Formulation

$$\frac{D_0\boldsymbol{\xi}}{Dt^2}+\delta\left(\frac{1}{\rho}\nabla p+\nabla\psi\right)=\delta\boldsymbol{N},$$

$$\frac{D_0}{Dt}\delta p-c_{\mathrm{s}}^2\frac{D_0}{Dt}\delta\rho=\delta[(\Gamma_3-1)(-\mathrm{div}\boldsymbol{F}+\Phi)],$$

$$\frac{D_0}{Dt}(\delta p)_{\mathrm{na}}=\delta[(\Gamma_3-1)(-\mathrm{div}\boldsymbol{F}+\Phi)].$$

$$\rho_0\frac{\partial^2\boldsymbol{\xi}}{\partial t^2}+2\rho_0(\boldsymbol{u}_0\cdot\nabla)\frac{\partial}{\partial t}\boldsymbol{\xi}+\mathscr{L}(\boldsymbol{\xi})=\rho_0\delta\boldsymbol{N}-\nabla(\delta p)_{\mathrm{na}}.$$

$$\boldsymbol{\xi}=\Re[\hat{\boldsymbol{\xi}}\exp(i\omega t)]=\Re\left[\breve{\boldsymbol{\xi}}\exp[i(\omega t-m\varphi)]\right],$$

$$-\omega^2\rho_0\hat{\boldsymbol{\xi}}+2i\omega\rho_0(\boldsymbol{u}_0\cdot\nabla)\hat{\boldsymbol{\xi}}+\mathscr{L}(\hat{\boldsymbol{\xi}})=\rho_0\delta\hat{\boldsymbol{N}}-\nabla(\hat{\delta p})_{\mathrm{na}}.$$

$$-\omega^2\rho_0\hat{\boldsymbol{\xi}}+2i\omega\rho_0(\boldsymbol{u}_0\cdot\nabla)\hat{\boldsymbol{\xi}}+\mathscr{L}(\hat{\boldsymbol{\xi}})=\rho_0\delta\hat{\boldsymbol{N}}-\nabla(\hat{\delta p})_{\mathrm{na}}.$$

$$\Im\left[-\omega^2\int\rho_0\hat{\boldsymbol{\xi}}^*\hat{\boldsymbol{\xi}}d^3r+2i\omega\int\rho_0\hat{\boldsymbol{\xi}}^*(\boldsymbol{u}_0\cdot\nabla)\hat{\boldsymbol{\xi}}d^3r\right]$$
$$=\Im\int\hat{\boldsymbol{\xi}}^*\cdot\left[\rho_0\delta\hat{\boldsymbol{N}}-\nabla(\hat{\delta p})_{\mathrm{na}}\right]d^3r,$$

$$\omega=\omega_0+i\omega_{\mathrm{i}},$$

$$-2\omega_{\mathrm{i}}\left[\omega_0\int\rho_0\hat{\boldsymbol{\xi}}^*\cdot\hat{\boldsymbol{\xi}}d^3r-i\int\rho_0\hat{\boldsymbol{\xi}}^*(\boldsymbol{u}_0\cdot\nabla)\hat{\boldsymbol{\xi}}d^3r\right]=\Im\int\hat{\boldsymbol{\xi}}^*\cdot\left[\rho_0\delta\hat{\boldsymbol{N}}-\nabla(\hat{\delta p})_{\mathrm{na}}\right]d^3r,$$

$$E=\frac{1}{2}\int\left[\omega_0^2\rho_0\hat{\boldsymbol{\xi}}^*\cdot\hat{\boldsymbol{\xi}}-i\omega_0\rho_0\hat{\boldsymbol{\xi}}^*(\boldsymbol{u}_0\cdot\nabla)\hat{\boldsymbol{\xi}}\right]dV.$$

$$-\omega_{\mathrm{i}}=\frac{\omega_0}{4E}\Im\int\hat{\boldsymbol{\xi}}^*\cdot\left[\rho_0\delta\hat{\boldsymbol{N}}-\nabla(\hat{\delta p})_{\mathrm{na}}\right]d^3r.$$

$$(-\omega_{\mathrm{i}})_{\mathrm{nonad}} = \frac{1}{4E}\Re\int \frac{\omega_0}{\omega_0 - m\Omega}\left(\frac{\delta\breve{T}}{T_0}\right)^{*}\delta(-\mathrm{div}\breve{\boldsymbol{F}} + \breve{\Phi})d^3r.$$

$$-\omega_{\mathrm{i}} = \frac{\omega_0}{4E}\Im\int \rho_0\hat{\boldsymbol{\xi}}^{*}\cdot\delta\hat{\boldsymbol{N}}d^3r.$$

$$(-\omega_{\mathrm{i}})_{\mathrm{viscosity}} = \frac{\omega_0}{4E}\Re\int \rho_0\frac{1}{\omega_0 - m\Omega}\left(\breve{u}_r^{*}\breve{N}_{1r} + \frac{4\Omega^2}{\kappa^2}\breve{u}_\varphi^{*}\breve{N}_{1\varphi} + \breve{u}_z^{*}\breve{N}_{1z}\right)d^3r.$$

Corotation resonance

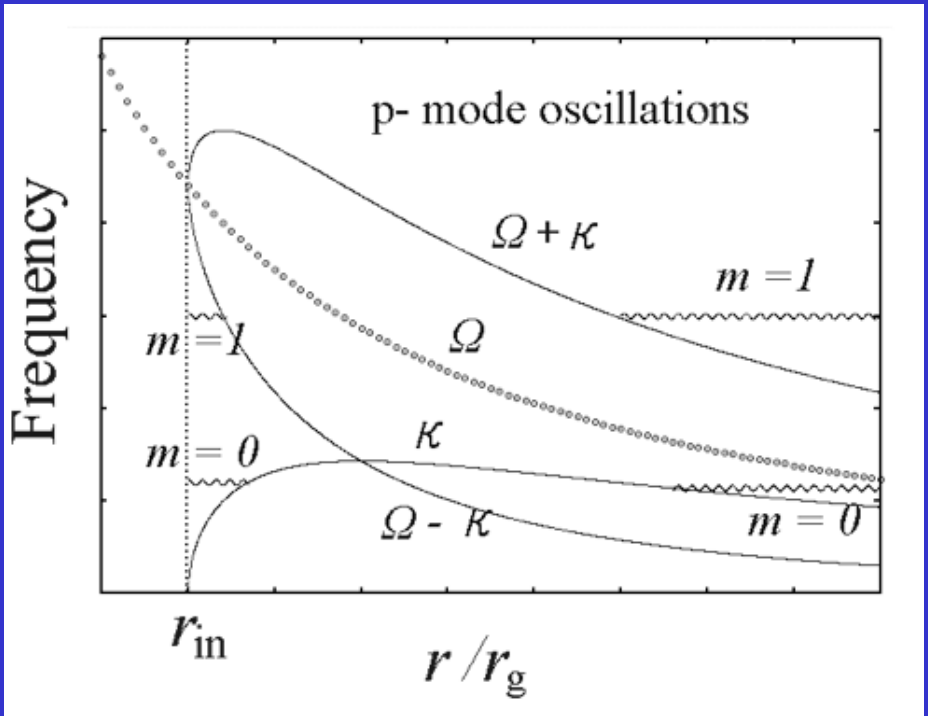

P-mode oscillations	grow
G-mode oscillations	damp
Vertical p-mode	damp

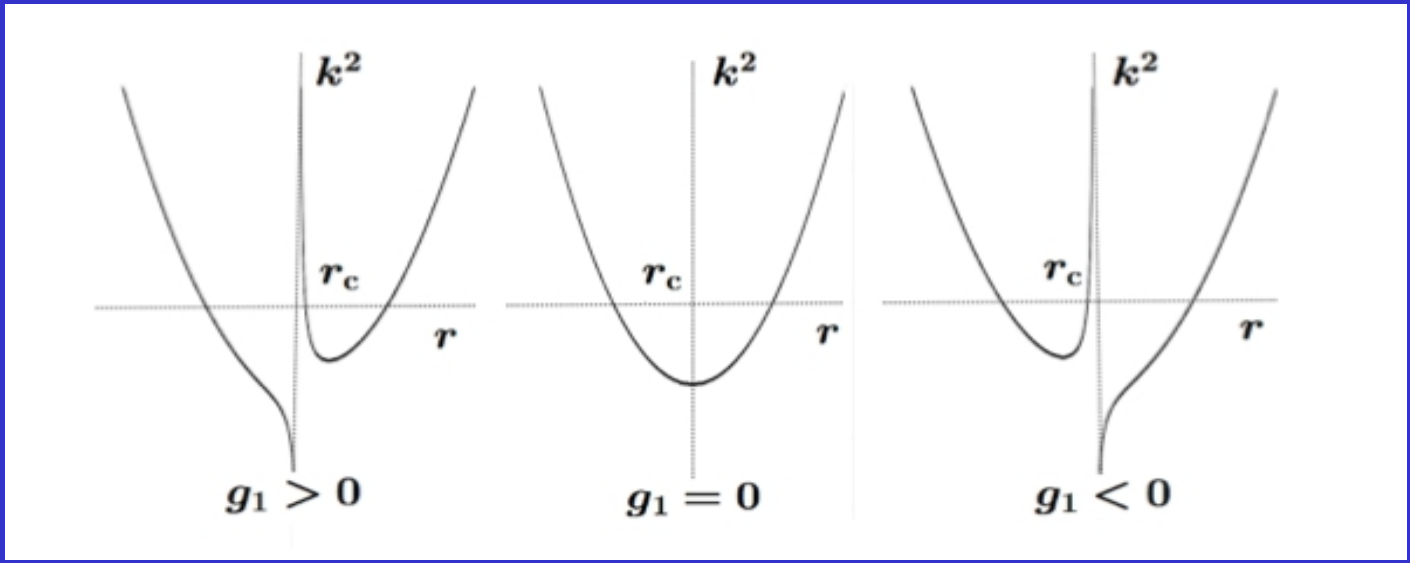

$$g_1 = \frac{d}{dr}\left[\frac{\kappa^2/2\Omega}{\rho_{00}}\right]_c.$$

vortensity gradient at corotation point

$$\mathrm{Sgn}(g_1) = \mathrm{Sgn}\left[\frac{d}{dr}\left(\frac{\kappa^2/2\Omega}{\rho_{00}}\right)\right]_{r_c}.$$

Entropy gradient がある場合

$$K^2 \sim -\frac{\kappa^2}{c_s^2} + 2m\Omega\frac{d}{rdr}\ln\left(\frac{\kappa^2}{2\Omega\Sigma_0}\frac{p_0}{\rho_0^{1/\gamma}}\right)\frac{1}{\tilde{\omega}} + \frac{m^2c_s^2}{r^2}\frac{d}{dr}\ln\left(\frac{p_0}{\rho_0^{1/\gamma}}\right)\frac{d\ln\Sigma_0}{dr}\frac{1}{\tilde{\omega}^2},$$

Overreflection at Corotation Resonance

Three Cases

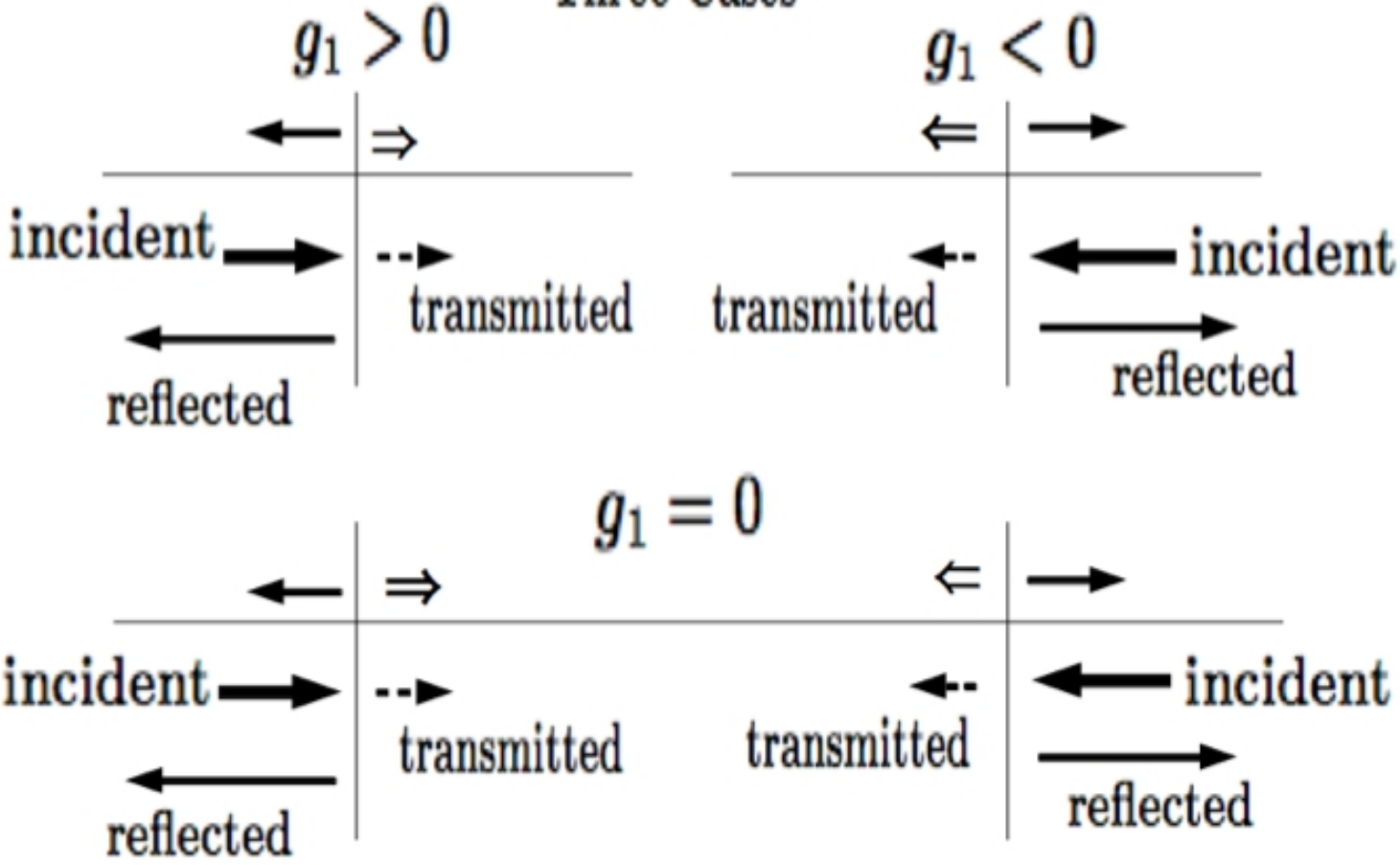

Rossby-type waves

5 .Wave – wave Resonant Instability

three-mode resonant interaction

(ω_1, m_1)

(ω_2, m_2)

(ω_D, m_D) – – –– disk deformartion

resonance condition

$$\omega_1 + \omega_2 + \Omega_D = 0$$

$$m_1 + m_2 + m_D = 0$$

instability condition

$$\left(\frac{E_1}{\omega_1}\right)\left(\frac{E_2}{\omega_2}\right) > 0$$

$$E_1 E_2 < 0 \quad \text{if } \omega_D = 0$$

Resonant Instability

$$(E_1/\omega_1)(E_2/\omega_2) > 0$$

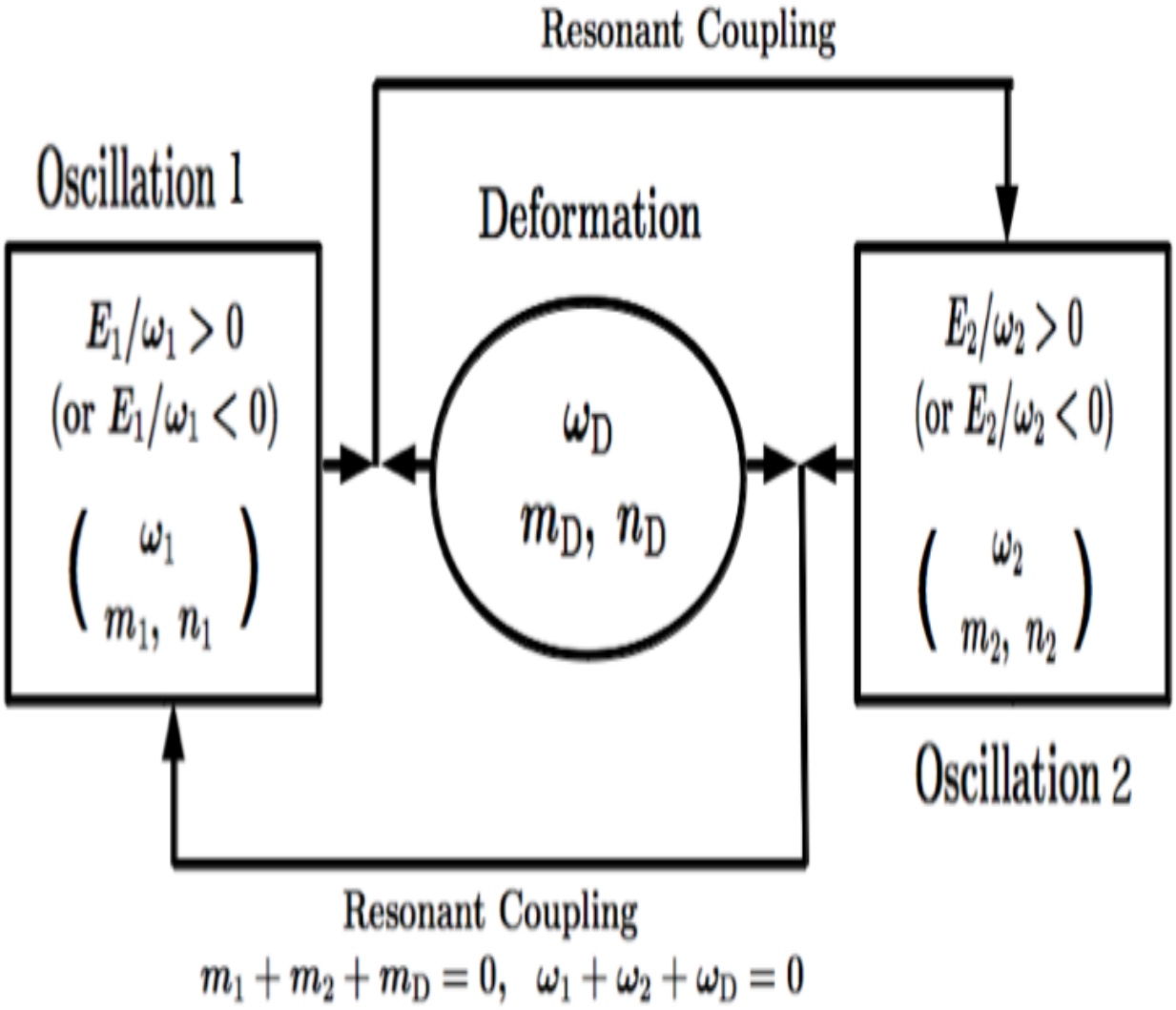

$$m_1 + m_2 + m_D = 0, \quad \omega_1 + \omega_2 + \omega_D = 0$$

Derivation of stability criterion

$$\boldsymbol{\xi}(\boldsymbol{r},t) = A_1\boldsymbol{\xi}_1(\boldsymbol{r},t) + A_2\boldsymbol{\xi}_2(\boldsymbol{r},t)$$
$$= \Re\left[A_1\check{\boldsymbol{\xi}}_1\exp[i(\omega_1 t - m_1\varphi)] + A_2\check{\boldsymbol{\xi}}_2\exp[i(\omega_2 t - m_2\varphi)]\right],$$

$$\rho_0\frac{\partial^2\boldsymbol{\xi}}{\partial t^2} + 2\rho_0(\boldsymbol{u}_0\cdot\nabla)\frac{\partial\boldsymbol{\xi}}{\partial t} + \mathscr{L}(\boldsymbol{\xi}) = \boldsymbol{C}(\boldsymbol{\xi},\boldsymbol{\xi}_{\mathrm{D}}),$$

$$C_k(\boldsymbol{\xi},\boldsymbol{\xi}_{\mathrm{D}}) = -\rho_0\xi_i\xi_{\mathrm{D}j}\frac{\partial^3}{\partial r_i\partial r_j\partial r_k}\psi_0 - \frac{\partial}{\partial r_j}\left(p_0\frac{\partial\xi_i}{\partial r_k}\frac{\partial\xi_{\mathrm{D}j}}{\partial r_i} + p_0\frac{\partial\xi_{\mathrm{D}i}}{\partial r_k}\frac{\partial\xi_j}{\partial r_i}\right)$$
$$+\frac{\partial}{\partial r_j}\left[(\Gamma_1-1)p_0\left(\frac{\partial\xi_j}{\partial r_k}\mathrm{div}\boldsymbol{\xi}_{\mathrm{D}} + \frac{\partial\xi_{\mathrm{D}j}}{\partial r_k}\mathrm{div}\boldsymbol{\xi}\right)\right]$$
$$+\frac{\partial}{\partial r_k}\left[(\Gamma_1-1)p_0\frac{\partial\xi_i}{\partial r_j}\frac{\partial\xi_{\mathrm{D}j}}{\partial r_i}\right] + \frac{\partial}{\partial r_k}\left[(\Gamma_1-1)^2 p_0\mathrm{div}\boldsymbol{\xi}\,\mathrm{div}\boldsymbol{\xi}_{\mathrm{D}}\right], \qquad (11.3$$

$$\boldsymbol{\xi}(\boldsymbol{r},t) = \Re\sum_{\mathrm{i}=1}^{2}A_{\mathrm{i}}(t)\hat{\boldsymbol{\xi}}_{\mathrm{i}}(\boldsymbol{r})\exp(\mathrm{i}\omega_{\mathrm{i}}\mathrm{t}) + \Re\sum_{\mathrm{i}}^{2}\left(\sum_{\alpha\neq1,2}\mathrm{A}_{\mathrm{i},\alpha}\hat{\boldsymbol{\xi}}_{\alpha}(\boldsymbol{r})\right)\exp(\mathrm{i}\omega_{\alpha}\mathrm{t})$$
+oscillating terms with other frequencies. (11.35)

$$\Re\, i\frac{2E_1}{\omega_1}\frac{dA_1}{dt} = \frac{1}{2}\Re\left[A_2(t)A_{\rm D}\left\langle \hat{\boldsymbol{\xi}}_1\cdot\boldsymbol{C}(\hat{\boldsymbol{\xi}}_2,\hat{\boldsymbol{\xi}}_{\rm D})\right\rangle \exp(i\Delta\omega t)\right],$$

$$\Re\, i\frac{2E_2}{\omega_2}\frac{dA_2}{dt} = \frac{1}{2}\Re\left[A_1(t)A_{\rm D}\left\langle \hat{\boldsymbol{\xi}}_2\cdot\boldsymbol{C}(\hat{\boldsymbol{\xi}}_1,\hat{\boldsymbol{\xi}}_{\rm D})\right\rangle \exp(i\Delta\omega t)\right].$$

$$-\frac{2E_1}{\omega_1}\frac{A_{1,\rm i}}{dt} = -\frac{1}{2}A_{2,\rm i}\Im(A_{\rm D}W),$$

$$-\frac{2E_2}{\omega_2}\frac{A_{2,\rm i}}{dt} = -\frac{1}{2}A_{1,\rm i}\Im(A_{\rm D}W),$$

$$W \equiv \left\langle \hat{\boldsymbol{\xi}}_1\cdot\boldsymbol{C}(\hat{\boldsymbol{\xi}}_2,\hat{\boldsymbol{\xi}}_{\rm D})\right\rangle = \left\langle \hat{\boldsymbol{\xi}}_2\cdot\boldsymbol{C}(\hat{\boldsymbol{\xi}}_1,\hat{\boldsymbol{\xi}}_{\rm D})\right\rangle.$$

$$\frac{d^2A_{1,\rm i}}{dt^2} = \frac{1}{16}\left(\frac{E_1E_2}{\omega_1\omega_2}\right)^{-1}\left[\Im(A_{\rm D}W)\right]^2 A_{1,\rm i}.$$

$$\frac{E_1E_2}{\omega_1\omega_2} > 0,$$

(instability condition)

Wave-wave resonant instability に関するコメント

1） magnetic fields 存在しても不安定の条件:

$$\frac{E_1 E_2}{\omega_1 \omega_2} > 0,$$

は変わらない。

2） 第三のモードの振幅を固定せず、相互作用によって第三のモードの振幅も変化するとすると、不安定の条件が満たされる場合、三つのモードが、相互に振幅を変えながら、振動する。

Pattern formation の問題

$$\frac{E_1}{\omega_1} A_{1,i}^2 - \frac{E_2}{\omega_2} A_{2,i}^2 = \text{const.}$$

$$\frac{E_1}{\omega_1} A_{1,i}^2 - \frac{E_D}{\omega_D} A_{D,i}^2 = \text{const.}$$

$$\frac{E_2}{\omega_2} A_{2,i}^2 - \frac{E_D}{\omega_D} A_{D,i}^2 = \text{const.},$$

6. Application of wave-wave resonant instability
(a) superhumps of dwarf novae

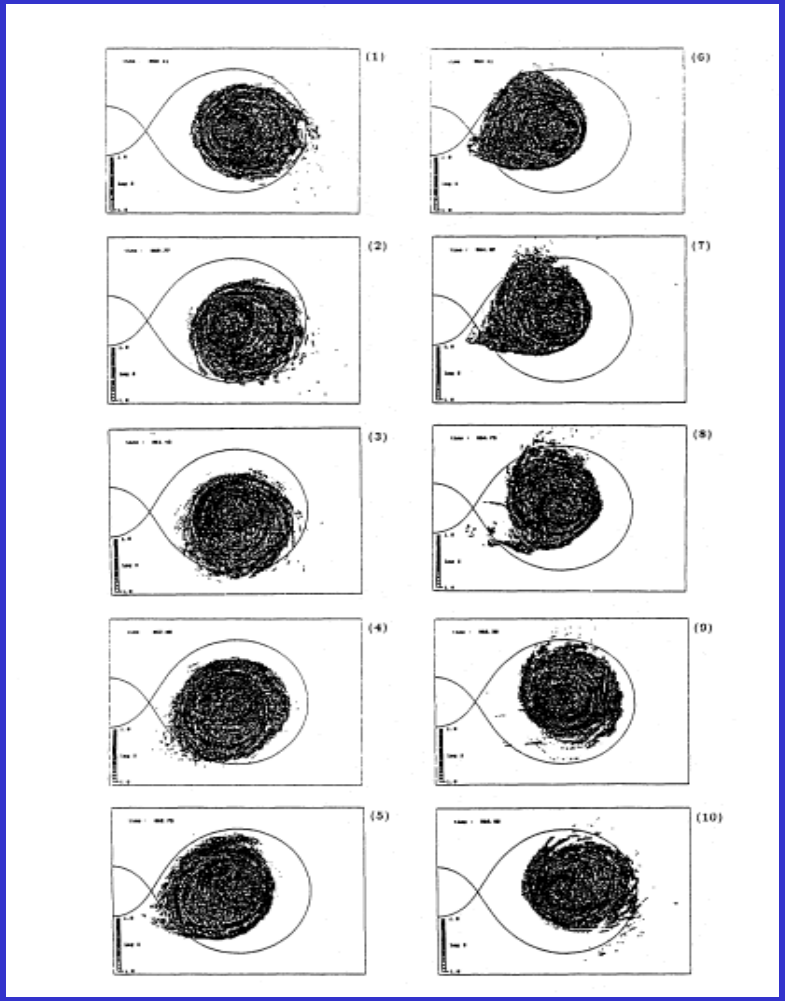

Hirose and Osaki (1990)

3 : 1 resonance

$$\Omega \simeq 3\Omega_{\rm orb}$$

Numerical simulations

Whitehurst 1988

Theoretical

Hirose and Osaki 1990 (particle)

Lubow 1991 (fluid)

w-w resonance model

A particular case of more general instability criterion

- ω_1-mode (one-armed (m=1) p-mode)
  (low-frequency precession mode)

$$(\omega - m\Omega)^2 > \kappa^2$$

$$\omega_1 - \Omega < -\kappa \quad \text{or} \quad \omega_1 < \Omega - \kappa$$

- ω_2-mode (p-mode with m_2)

$$\omega_2 - 2\Omega < -\kappa \quad \text{or} \quad \omega_2 < 2\Omega - \kappa$$

- ω_D-mode

$$\frac{E_1}{\omega_1}\frac{E_2}{\omega_2} > 0$$

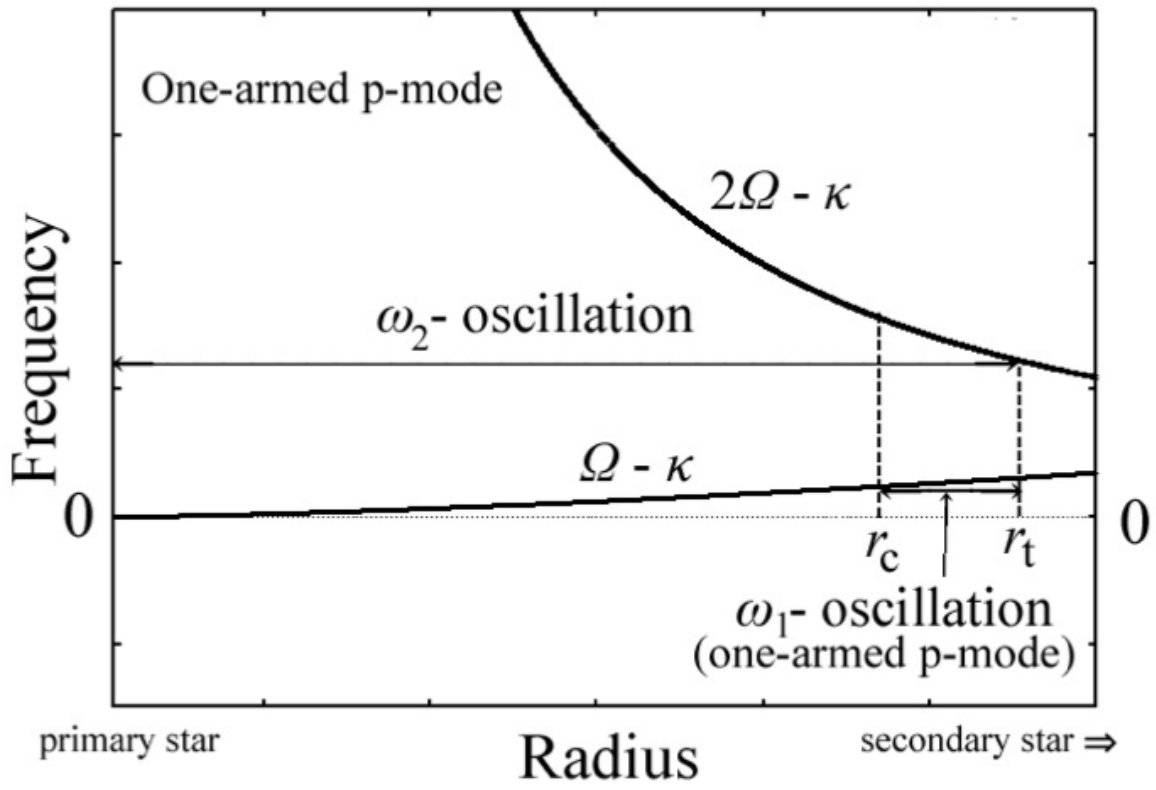

Schematic diagram showing frequencies and propagation regions of the ω_1- and ω_2-oscillations in the case where the ω_1-oscillation is one-armed low-frequency p-mode oscillation, and the ω_2-oscillation is two-armed p-mode oscillation. The scales of coordinates are arbitrary, and are not linear. The one-armed p-mode oscillation is trapped between r_c and r_t. The inside is the evanescent region. The ω_2-oscillation can propagate inside r_t.

from resonant condition $\omega_1 + \omega_2 + \omega_D = 0$ and definition $\omega_D = n\Omega_{orb}$:

$$(\Omega - \kappa)_c + (m_2\Omega - \kappa)_t + n\Omega_{orb} = 0.$$

$$\Omega_t = \frac{n}{1-m_2}\Omega_{orb}$$

if $m_2 = 2$ is adopted, another resonant condition: $m_1 + m_2 + m_D = 0$ requires $m_D = -3$.

A strong tidal wave with $m_D = -3$ has

$$\omega_D = -3\Omega_{orb}, \text{ i.e., } n = -3.$$

That is, the condition of resonant instability is

$$\Omega_t : \Omega_{orb} = 3 : 1$$

6. Application of wave-wave resonant instability

(b) self-trapped g-mode excitation in warped disks

Warped Disk

$$m_D = -1, n_D = 1 \text{ and } \omega_D = 0 \quad \text{(warped disk)}$$

$$m_1 = 1,\ n_1 = 0,\ \omega_1 > 0, \text{ and } E_1/\omega_1 < 0 \quad \text{(one armed p mode).}$$

$$m_2 = 0,\ n_2 = 1,\ \omega_2 < 0, \text{ and } E_2/\omega_2 < 0 \quad \text{(axisymmetric g mode).}$$

$n = 1$ $m = 0$ (axisymmetric g-mode)

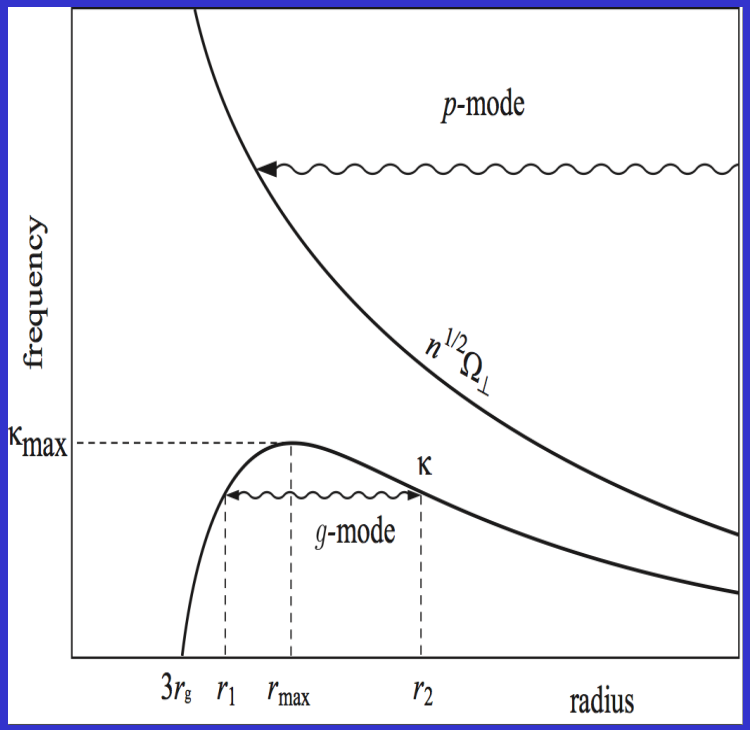

$n = 0$ (p-mode) with $m = 1$

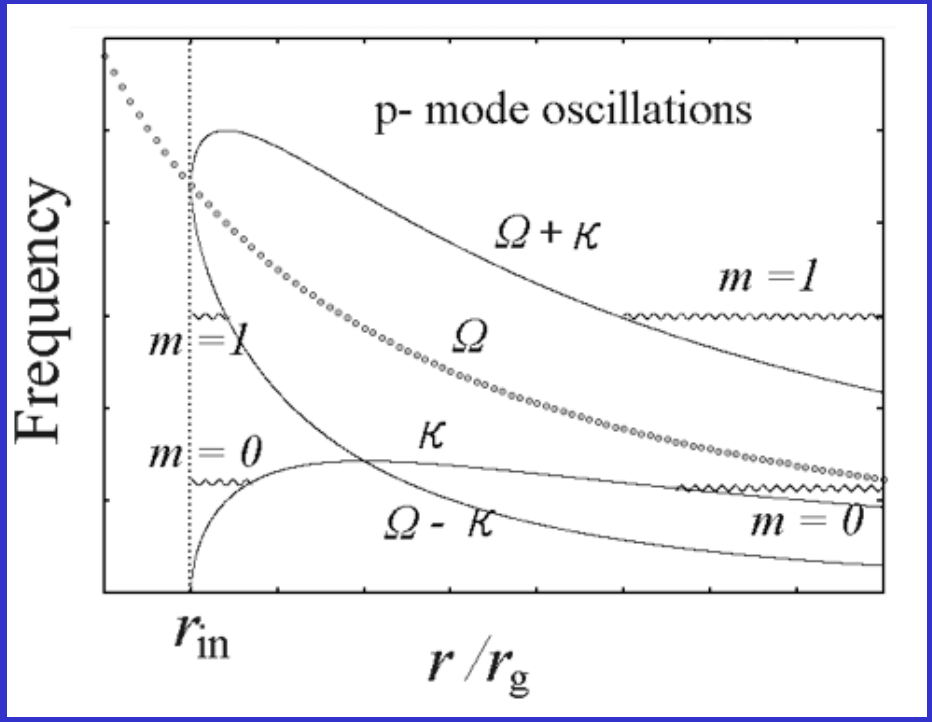

Self-trapping of g-mode oscillations and their excitationに関する歴史

Self-trapping の存在の指摘：

Okazaki, Kato, Fukue 1987 ：

QPOs の起源ではないか？

Nowak, Wagoner, Begelman, Lehr 1997 :

Warp resonance で振動の励起可能:

Kato 2004, 2008; Ferreria, Ogilvie 2008;
Oktariani, Okazaki, Kato 2008
Kato 2013 (一般的な励起条件導出)

Vertical mag fields があると trapping なくなる

Fu and Lai 2009:

Toroidal fields があれば trapping ある

Dewberry, Latter, Ogilvie 2019

QPOs の１つの有力な候補：

現実的なWarped disk での励起を実証した？
Ogilvie のグループ 2019？

7. Twin QPOs の説明に使えそうなその他のモデル

- P-mode oscillations excited by corotation resonance

  3 : 2 QPOs の説明に適したモデル

- Two-armed, c-mode Oscillations in two-armed deformed disks

  kHz QPOs の correlated freq. change の説明に適している。

7.1 P-mode oscillations excited by corotation resonance

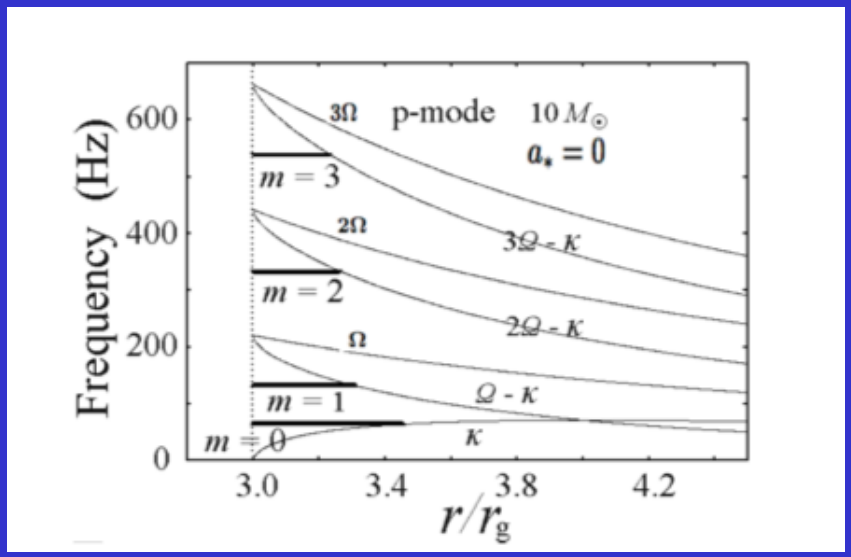

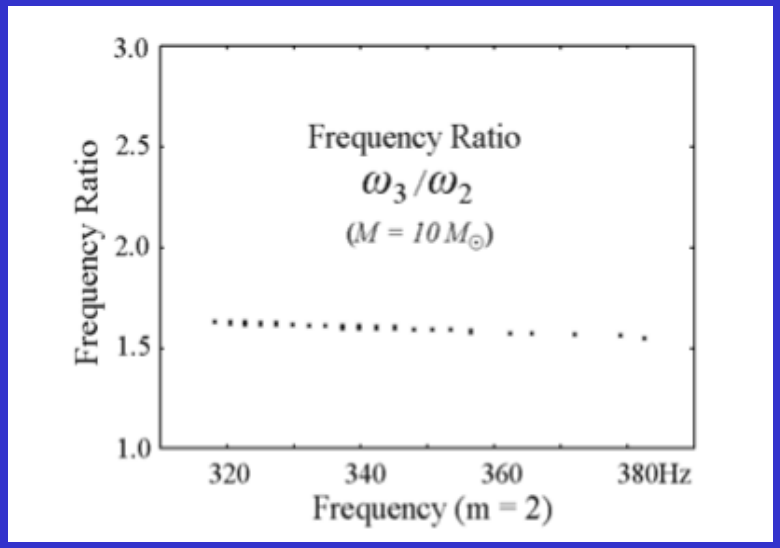

利点： 1) insensible to parameter changes

2) close to 3 : 2 → BH QPOs

3) excited by corotation resonance

Lai, Tsang 2009: Horak, Lai 2013

7.2 Two-armed (m=2) c-mode (n=1) oscillations

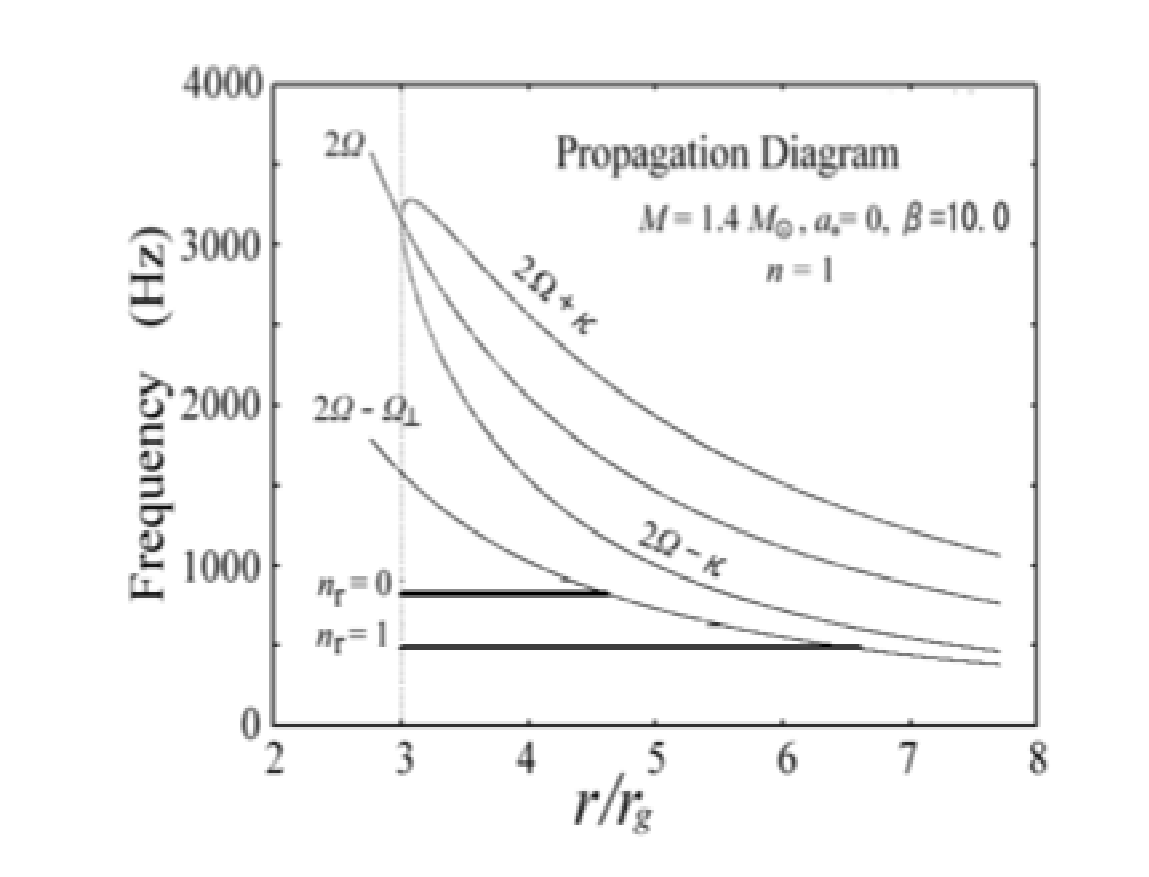

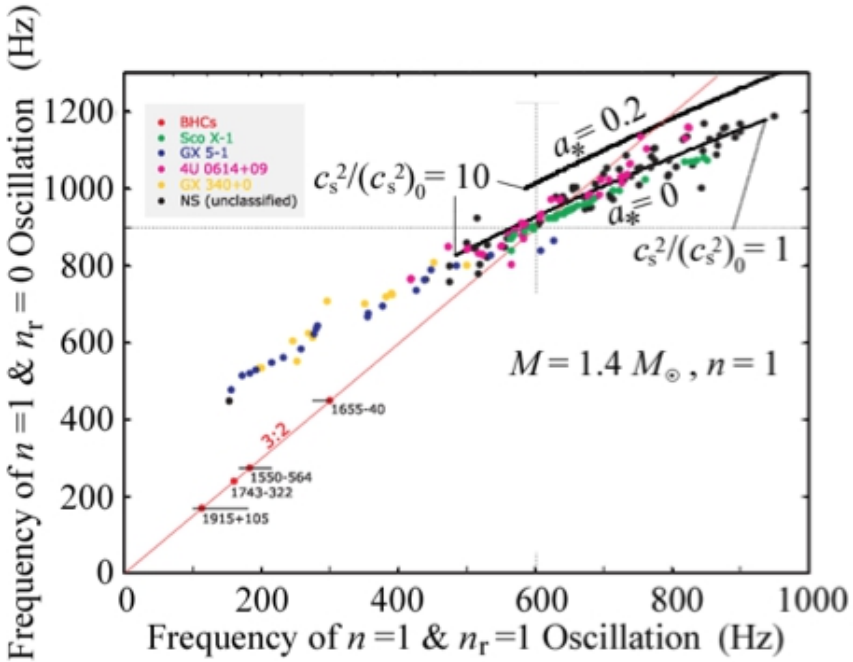

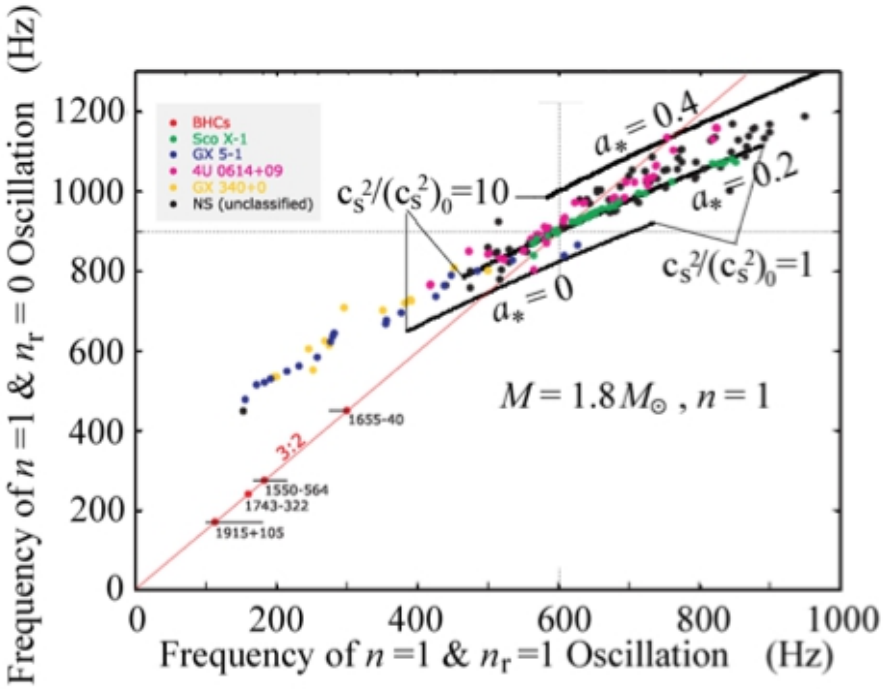

特徴： 1) close to pairs of kHz QPOs

2) to be excited by two-armed deformed disks

全体に関する参考文献:

S. Kato 2016, Oscillations of Disks (Springer)